Raman Scattering Characterization of $Mo_xW_{1-x}S_2$ Layered Mixed Crystals

M. Sigiro*

Department of Physics Education, Faculty of Education and Teacher Training, Universitas HKBP Nomensen, Medan 20234, Indonesia

(Received August 31, 2016; in final form January 5, 2017)

A series of $Mo_xW_{1-x}S_2$ ($0 \leq x \leq 1$) layered mixed crystals was grown by the chemical vapor transport method. A systematic study of these crystals was then conducted using the Raman scattering measurements. The peaks of the two dominant first-order Raman-active modes, A_{1g} and E^1_{2g}, and of several second-order bands are observed from 150 cm^{-1} to 500 cm^{-1}. The peaks corresponding to A_{1g} mode show one-mode type behavior, whereas the peaks of E^1_{2g} mode demonstrate two-mode type behavior for the entire series. These results can be explained by the atomic displacements of each mode. For A_{1g} mode, only S atoms vibrate, thereby resulting in a one-mode type behavior for the mixed crystals. For E^1_{2g} mode, metal and S atoms vibrate. The mass difference in the vibrating Mo and W cations causes the two-mode type behavior of E^1_{2g} mode. In addition, the largest asymmetry and broadening of A_{1g} mode for $Mo_{0.5}W_{0.5}S_2$ is attributed to random alloy scattering.

DOI: 10.12693/APhysPolA.131.259

PACS/topics: Raman-active mode, layered mixed crystal, atomic displacement, chemical-vapor transport method

1. Introduction

Layered semiconductors TX_2 are receiving significant interest because of their structural properties. MoS_2 is an important member of layered-type transition metal dichalcogenides, which have a VI-group layer-type structure [1] MX_2 (or WX_2), where M = Mo or W, and X = S or Se. The "layered" structure of MoS_2 is formed by a graphene-like hexagonal arrangement of Mo and S atoms stacked together to achieve S–Mo–S sandwiches, which are coordinated in a triangular prismatic fashion. The S–Mo–S sandwiches are bonded together by weak Van der Waals forces [2]. Layered semiconductors are potential candidates in various important technologies, such as solid lubricants [3–5], photovoltaic and polymer solar cells [6–10], and hydrosulphurization catalysts [11]. The possibility of obtaining MoS_2 by exfoliation of multilayered MoS_2 into single-layered MoS_2nanosheets, followed by a Li-intercalation and exfoliation method [12, 13] allowed the solution-based production and thin-film fabrication of MoS_2 sheets, which are applicable in high-performance electronics. In addition, a high in-plane carrier mobility of ≈ 200 cm^2 V^{-1} s^{-1} to 500 cm^2 V^{-1} s^{-1} and superior mechanical properties of the MoS_2 nanosheets have made them promising materials for various applications in electronic devices [14–17]. Given these versatile properties, many researchers have investigated the utilization of MoS_2 as a semiconducting channel material for high-performance unipolar or ambipolar field-effect transistors [14, 18–21]. Over the last two decades, several papers concerning the preparation and characterization of $Mo_xW_{1-x}S_2$ compounds using various methods have been published [22–26]. The X-r has layered-type structure with hexagonal symmetry [22, 23]. The thermal decomposition of thiometallate solid solutions $(NH_4)_2Mo_{1-x}W_xS_4$ in an inert or hydrogen atmosphere yields $Mo_xW_{1-x}S_2$ nanotubes and related structures [24–26]. Using piezoreflectance measurements in the vicinity of the direct band edge, the transition energies were found to vary smoothly with the W composition x, thereby indicating that the natures of the direct band edges are similar for the $Mo_xW_{1-x}S_2$ compounds [23].

In this report, we present a systematic Raman scattering study of a series of $Mo_xW_{1-x}S_2$ layered mixed crystals grown using chemical-vapor transport method. The peaks of the two dominant first-order Raman-active modes, A_{1g} and E^1_{2g}, and several second-order (SOR) bands were observed. Polarization-dependent measurements in the backscattering configuration were performed to determine the positions of A_{1g} and E^1_{2g} modes at different W composition x. The peaks that correspond to A_{1g} mode show one-mode type behavior, whereas the peaks of E^1_{2g} mode demonstrate two-mode type behavior for the entire series. The composition-dependent behaviors of A_{1g} and E^1_{2g} modes are discussed.

2. Experimental

Solid solutions of $Mo_xW_{1-x}S_2$ single crystals were grown using chemical-vapor transport method with Br_2 as a transport agent. The total charge used in each growth experiment was approximately 10 g. The W and Mo materials were added in such manner that the W composition x changes with respect to increases of the Mo from 0 to 1 with a composition step size $\Delta x = 0.1$. Prior to crystal growing, the powdered compounds of the series were prepared from the elements (Mo: 99.99%,

*e-mail: mulasigiro@gmail.com

W: 99.95%, and S: 99.999%) by reaction at 1000 °C for 10 days in evacuated quartz ampoules, which was sealed at 10^{-6} Torr. The ampoule, which contained Br_2 (≈ 5 mg cm^{-3}), was then placed in a three-zone furnace, and the charge was pre-reacted for 24 h at 800 °C with the growth zone at 950 °C, thereby preventing the transport of the product. The temperature of the furnace was increased slowly to avoid any possible explosion caused by exothermic reaction between the elements. The furnace was then equilibrated to achieve a constant temperature across the reaction tube, and then programmed over 24 h to produce the temperature gradient at which single-crystal growth occurred. Optimal results were obtained at a temperature gradient of approximately 960 °C to 930 °C. Single crystalline platelets up to 10×10 mm^2 surface area and 2 mm in thickness were obtained. We do not expect the two solid solutions to be miscible.

The Raman measurements were performed at room temperature using the backscattering configuration on a Renishaw micro-Raman system with 1800 grooves/mm grating (Fig. 1). An optical microscope with a 50× objective was used to focus the laser beam on the sample placed on an $X-Y$ motorized sample stage. A linearly polarized Ar^+ laser beam (514.5 nm excitation line) with a power of $\approx$ 1.5 mW was focused into a spot size of ≈ 5 μm in diameter. Prior to measurement, the system was calibrated using the 520 cm^{-1} Raman peak of a polycrystalline Si. The time of acquisition of a particular spectral window was optimized for individual sample measurements. Fifty accumulations were performed to obtain a spectrum.

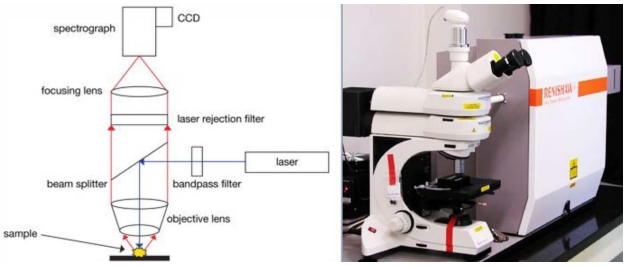

Fig. 1. Schematic diagram of the setup for Raman spectroscopy system.

3. Results and discussion

Polarization-dependent measurements in the backscattering configuration were performed to determine the position of A_{1g} and E^1_{2g} modes accurately, as well as the SOR band located in the vicinity of E^1_{2g} of the W-containing samples. The Porto notation method [27] was used for the designation of the crystal and polarization directions. The [1 0 0], [0 1 0], and [0 0 1] crystallographic axes are denoted by the letters X, Y, and Z, respectively. The notation $Z(XX)\bar{Z}$ means that the direction of incident radiation is along the Z, the first and second terms in the bracket denotes the polarization of the incident and scattered light, respectively, and $\bar{Z}$ represents the direction of scattered light. For $Z(XX)\bar{Z}$ configuration, the analyzer, which was placed just in front of the charge-coupled device (CCD) camera, was set to have polarization axis that is parallel to the polarization of the incident linearly polarized laser beam. A fine adjustment in the orientation of the [1 0 0] crystallographic axis of the sample to the $\boldsymbol{E}$ vector of the incident linearly polarized laser beam was performed by maximizing the intensity of the A_{1g} mode. The $Z(XX)\bar{Z}$ configuration was obtained simply by placing the half-wavelength plate directly between the analyzer and the CCD camera.

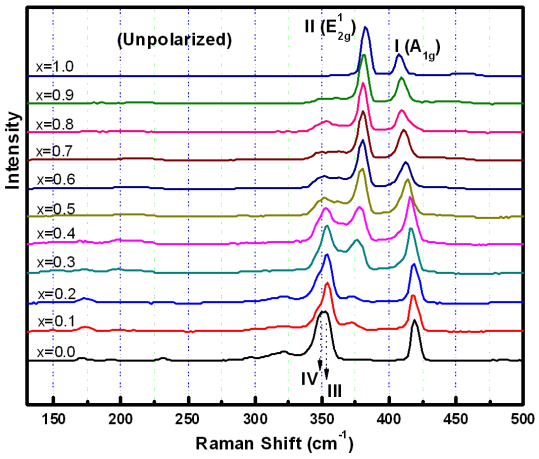

Fig. 2. Unpolarized Raman spectra between 150 and 500 cm^{-1} of $Mo_xW_{1-x}S_2$ layered mixed crystals. The dotted lines guided by eyes show position dependence of the peaks with Mo compositions x.

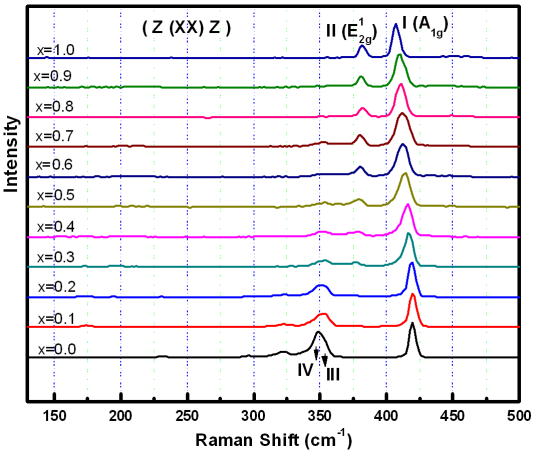

Fig. 3. Polarized Raman spectra between 150 and 500 cm^{-1} of $Mo_xW_{1-x}S_2$ layered mixed crystals. The dotted lines guided by eyes show position dependence of the peaks with Mo compositions x.

The results of polarization-dependent Raman spectra between 150 and 500 cm^{-1} of several $Mo_xW_{1-x}S_2$ mixed crystals are shown in Figs. 2 and 3. The intensity of the Raman lines in $Z(XX)\bar{Z}$ and $Z(XY)\bar{Z}$ configurations differ significantly, showing the strong polarization dependence of the first-order Raman-active modes. In

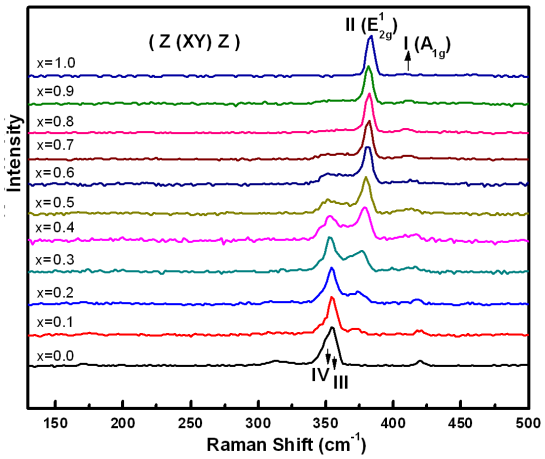

Fig. 4. Raman spectra (between 150 and 500 cm^{-1}) of $Mo_xW_{1-x}S_2$ layered mixed crystals for polarized added half wave plate. The dotted lines guided by eyes show position dependence of the peaks with Mo compositions x.

this wave number range, for 2H-MoS_2 single crystal, the peak denoted by I, which corresponds to A_{1g} mode, is detected for $Z(XX)\bar{Z}$configuration and quenched almost completely for that of $Z(XY)\bar{Z}$ configuration. The lower lying peak denoted by II is associated with E^1_{2g} mode and observed both for $Z(XX)\bar{Z}$ and $Z(XY)\bar{Z}$ polarization configurations. Furthermore, the measured intensities of peak II for both $Z(XX)\bar{Z}$ and $Z(XY)\bar{Z}$ polarization show very similar values. The obtained results, together with the strong polarization dependence, are consistent with the selection rules of A_{1g} and E^1_{2g} modes as given by the Raman scattering tensors [28]. For the 2H-WS_2 sample, a similar polarization behavior for higher wave-number peak I is observed and assigned as the A_{1g} mode. The lower lying structure is determined to be composed of two peaks at 356 cm^{-1} (designated as III) and 352 cm^{-1} (designated as IV) in the $Z(XX)\bar{Z}$ configuration. A clear resolution of this structure can be seen in the unpolarized Raman spectrum of 2H-WS_2 (Fig. 2), as well as in the $Z(XY)\bar{Z}$ configuration in the polarized spectra (Fig. 3). The relative intensities for peaks III and IV in the $Z(XY)\bar{Z}$ configuration are larger than that of the $Z(XX)\bar{Z}$ configuration. This observation agrees with that reported by Sekine et al. [29]. Hence, the peak at 356 cm^{-1} is assigned as the E^1_{2g} mode, whereas the peak at 352 cm^{-1} is attributed to a SOR band. For the mixed $Mo_xW_{1-x}S_2$ samples, the assignment of peaks I and II can be facilitated by comparing their locations and polarization dependence with that of the binary end crystals. The relation of the relative intensities of peaks III and IV in the polarized Raman spectra were utilized for the assignment (Figs. 3 and 4).

Figure 4 shows the Raman spectra from 150 cm^{-1} to 500 cm^{-1} of $Mo_xW_{1-x}S_2$. From top to bottom, the value of the W composition x increases from 0 to 1 with a composition step size $\Delta x = 0.1$ according to the stoichiometry of the constituent elements W and Mo. With the increase in W composition, peak I moves to higher wave number. By contrast, as the value of x increases, peak II shifts to lower wave number with reduced peak intensity. In addition, with the increase in W composition, on the lower wave number side of the Raman spectra of $Mo_xW_{1-x}S_2$, two additional peaks (III and IV) appear. Both of these additional peaks demonstrate blue shift and become the dominant peaks at higher x values. An alloy disorder-related peak [30], which is positioned between peaks II and III, is also observed for the mixed ternary $Mo_xW_{1-x}S_2$ samples.

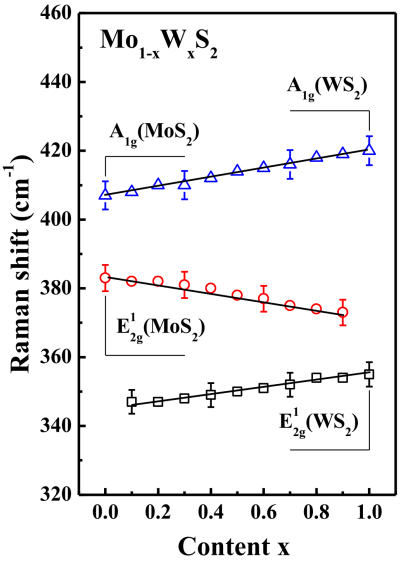

Fig. 5. The dependence of the wave numbers of the Raman-active modes on the composition of $Mo_xW_{1-x}S_2$ layered mixed crystals.

The dependences of the wave numbers of the Raman-active modes on the composition of $Mo_xW_{1-x}S_2$ layered mixed crystals are shown in Fig. 5. For the A_{1g} mode, a one-mode behavior is the most typical, whereas for the E^1_{2g} mode, a two-mode behavior is observed. These experimental results can be explained satisfactorily on the basis of the atomic displacements for each mode. In the A_{1g} mode, only S atoms vibrate, thereby resulting in a one-mode type behavior for the mixed crystals. In the E^1_{2g} mode, metal atoms vibrate, as well as S atoms (Fig. 2). The atomic weight of W atom is 1.92× larger than that of Mo atom, and this mass difference most probably causes two-mode type behavior of E^1_{2g} mode. These composition dependences are often seen in the Raman spectra of solid solutions with no ordered distribution of the constituent atoms [31, 32]; hence, the mixed crystals cannot have an ideal periodic lattice. As the composition of W increases, the disorder effect increases in the layered mixed crystals of $Mo_xW_{1-x}S_2$, and the intensities of the modes related to 2H-MoS_2 decreases, whereas the 2H-WS_2-associated modes increase. This finite periodicity in the mixed crystals relaxes the $q = 0$ Raman selection

rule, thereby leading to the broadening and asymmetry of the Raman line shape. Symmetric phonon line of the A_{1g} mode for pure 2H-MoS_2 and 2H-WS_2 become asymmetric for $Mo_xW_{1-x}S_2$ mixed crystals.

Line shape analysis of the Raman spectra under A_{1g} mode for MoS_2, $Mo_{0.5}W_{0.5}S_2$, and WS_2 layered crystals; the inset in MoS_2 represents the W composition dependence of linewidth broadening of A_{1g} mode for the $Mo_xW_{1-x}S_2$ layered mixed crystals. Similar broadening and asymmetry of the phonon lines were previously observed in $TlGa_xIn_{1-x}S_2$ layered mixed crystals [33]. The inset of $Mo_{0.5}W_{0.5}S_2$ shows the composition dependence of the full width at half maximum (FWHM) for A_{1g} mode. The FWHM values of the corresponding modes for MoS_2 layered crystals were higher than those for WS_2 crystals. In addition, as expected, the FWHM dependence is maximal at $x = 0.5$, which corresponds to the maximum substitution disorder in the mixed crystals.

4. Conclusions

The Raman spectra of $Mo_xW_{1-x}S_2$ layered mixed crystals were investigated for a wide range of composition ($0 \leq x \leq 1$). The peaks of the two dominant first-order Raman-active modes, A_{1g} and E^1_{2g}, and several SOR bands were observed between 150 cm^{-1} and 500 cm^{-1}. The peaks, which correspond to A_{1g} mode, show one-mode type behavior,whereas the peaks of E^1_{2g}mode demonstrate two-mode type behavior for the entire series. These results are explained on the basis of the atomic displacements for each mode. For A_{1g} mode, only S atoms vibrate, thereby resulting in a one-mode type behavior for the mixed crystals. By contrast, for the E^1_{2g} mode, metal atoms vibrate, as well as S atoms. The mass difference of the vibrating Mo and W cations causes the two-mode type behavior of the E^1_{2g} mode. The largest FWHM value and asymmetry of A_{1g} mode, which are due to crystal disorder, are found at $x = 0.5$.

Acknowledgments

The author acknowledge the support of Prof. Ying Sheng Huang and Prof. Ching Hwa-Ho for providing experimental facilities and discussions in Department of Electronic Engineering National Taiwan University of Science and Technology.

References

[1] J.A. Wilson, A.D. Yoffe, *Adv. Phys.* **18**, 193 (1969).

[2] E.S. Kadantsev, P. Hawrylak, *Solid State Commun.* **152**, 909 (2012).

[3] J.M. Martin, C. Donnet, J.L. Mogne, *Phys. Rev. B* **48**, 10583 (1993).

[4] M. Yanagisawa, *Wear* **168**, 167 (1993).

[5] P.D. Fleuschauer, *Thin Solid Films* **154**, 309 (1987).

[6] H. Tributsch, *Z. Nat.forsch. A* **32**, 972 (1977).

[7] K.K. Kam, B.A. Parkinson, *J. Phys. Chem.* **86**, 463 (1982).

[8] S.J. Li, J.C. Bernede, J. Pouze, M. Jamali, *J. Phys. Condens. Matter* **8**, 2291 (1996).

[9] A. Jager-Waldau, M. Lux-Steiner, R. Jager-Waldau, R. Burkhardt, E. Bucher, *Thin Solid Films* **189**, 339 (1990).

[10] Jin-Mun Yun, Yong-Jin Noh, Jun-Seok Yeo, Yeong-Jin Go, Seok-In Na, Hyung-Gu Jeong, Juhwan Kim, Sehyun Lee, Seok-Soon Kim, Hye Young Koo, Tae-Wook Kim, Dong-Yu Kim, *J. Mater. Chem. C* **1**, 3777 (2013).

[11] P. Grange, B. Delmon, *J. Less-Common Met.* **36**, 353 (1974).

[12] W.M.R. Divigalpitiya, S.R. Morrison, R.F. Frindt, *Thin Solid Films* **186**, 177 (1990).

[13] Z. Zeng, Z. Yin, X. Huang, H. Li, Q. He, G. Lu, F. Boey, H. Zhang, *Angew. Chem. Int. Ed.* **50**, 11093 (2011).

[14] B. Radisavljevic, A. Radenovic, J. Brivio, V. Giacometti, A. Kis, *Nat. Nanotechnol.* **6**, 147 (2011).

[15] A. Ayari, E. Cobas, O. Ogundadegbe, M.S. Fuhrer, *J. Appl. Phys.* **101**, 014507 (2007).

[16] X. Huang, Z. Zeng, H. Zhang, *Chem. Soc. Rev.* **42**, 1934 (2013).

[17] M. Chhowalla, H.S. Shin, G. Eda, L.-J. Li, K.P. Loh, H. Zhang, *Nat. Chem.* **5**, 263 (2013).

[18] H. Li, Z. Yin, Q. He, H. Li, X. Huang, G. Lu, D.W.H. Fam, A.L.Y. Tok, Q. Zhang, H. Zhang, *Small* **8**, 63 (2012).

[19] Z. Yin, H. Li, H. Li, L. Jiang, Y. Shi, Y. Sun, G. Lu, Q. Zhang, X. Chen and H. Zhang, *ACS Nano***6**, 74 (2012).

[20] Y. Zhang, J. Ye, Y. Matsuhashi, Y. Iwasa, *Nano Lett.* **12**, 1136 (2012).

[21] V. Podzorov, M.E. Gershenson, C. Kloc, R. Zeis, E. Bucher, *Appl. Phys. Lett.* **84**, 3301 (2004).

[22] S.K. Srivastava, T.K. Mandal, B.K. Samantaray, *Synth. Met.* 90, 135 (1997).

[23] J.A. van Vechten, T.K. Bergstresser, *Phys. Rev. B* **1**, 3351 (19701).

[24] C. Thomazeau, C. Geantet, M. Lacroix, V. Harlé, S. Benazeth, C. Marhic, M. Danot, *J. Solid State Chem.* **160**, 147 (2001).

[25] C. Thomazeau, C. Geantet, M. Lacroix, M. Danot, V. Harlé, P. Raybaud, *Appl. Catal. A Gen.* **322**, 92 (2007).

[26] M. Nath, K. Mukhopadhyay, C.N.R. Rao, *Chem. Phys. Lett.* **352**, 163 (2002).

[27] T.C. Damen, S.P.S. Porto, B. Tell, *Phys. Rev.* **142**, 570 (1966).

[28] R. Loudon, *Adv. Phys.* **13**, 423 (1964).

[29] T. Sekine, T. Nakashizu, K. Toyoda, K. Uchinokura, E. Matsuura, *Solid State Commun.* **35**, 371 (1980).

[30] S. Ould Saad Hamady, N. Dupuis, J. Décobert, A. Ougazzaden, *J. Cryst. Growth* **310**, 4741 (2008).

[31] M. Ishii, M. Saeki, *Solid State Commun.* **67**, 895 (1988).

[32] I.F. Chang, S.S. Mitra, *Adv. Phys.* **20**, 359 (1971).

[33] N.M. Gasanly, N.S. Yuksek, *Acta Phys. Pol. A* **108**, 997 (2005).